High-purity hybrid structural colors by enhancing optical absorption of organic dyes in resonant cavity

Zhengmei Yang,[1,2,#] Chengang Ji,[1,#] Qingyu Cui,[1] and L. Jay Guo[1,*]

[1] Department of Electrical Engineering and Computer Science, University of Michigan, Ann Arbor, Michigan 48109, USA

[2] School of Physics and Electronics, State Key Laboratory of Advanced Design and Manufacturing for Vehicle Body, Hunan University, Changsha 410082, China

[#] These authors contribute equally to this work.

[*] Corresponding author: guo@umich.edu

Abstract

This work presents a novel approach of incorporating an ultrathin dye film into a classic dielectric-absorber-dielectric-metal resonator configuration for generating high-purity reflective structural colors. Utilizing a thin film of organic dye having the same color as the targeted reflection color as a part of the cavity layer in the structure, its absorption at complementary color wavelengths is significantly enhanced due to the strong cavity resonances, hence reflection at the unwanted wavelengths strongly suppressed, leading to the improved purity of the desired reflective color. This design principle can be applied to create

essentially all colors, and was demonstrated by experiment to produce high-purity blue and red colors. In addition, the fabricated device exhibits outstanding stability under UV exposure without additional protections compared to traditional organic pigments. The proposed method in this work largely simplifies the design process of high-purity structural colors, which paves the way for more potential applications in various fields.

Keywords: reflective structural colors; Fabry-Pérot cavity; organic dyes; resonant optical absorption; interference effect

Introduction

Structural colors employing optical resonant properties in nanostructures have evolved rapidly in recent years due to their great promise in a broad range of applications such as color printing,[1-4] decorative power-generating panel,[5, 6] light-emitting diodes (LEDs),[7] display/imaging devices,[8-10] and high-color-purity pigments.[11, 12] In contrast to the existing color filters or coatings based on conventional organic dyes or pigments, which are vulnerable to various damages, e.g., when subjecting to long time ultraviolet (UV) exposure and high temperature, and usually require micrometer-scale thickness to produce distinctive colors, structural color filters offer unique advantages including high resolution, high brightness, slim dimension, long-term stability, and great tunability and scalability.[1] In the past decade, various systems such as metal-insulator-metal (MIM),[13-15] hole-array,[16] nano-grating,[17, 18] all-metallic,[19] and all-dielectric[4, 20-22] structures using different materials including aluminum (Al),[13, 23] silver (Ag),[15, 24] gold (Au),[14] copper (Cu),[25] silicon (Si),[20] and titanium oxide (TiO_2)[21] have been intensively studied to produce wide-gamut structural

colors utilizing plasmon resonance,[26] guided-mode resonance (GMR)[18] or Mie resonance.[27] However, the fabrications of these color filters require time-consuming, high-cost, and complicated nano-patterning procedures such as e-beam lithography and focused ion beam milling, which greatly limits their mass production and large-area applications. Therefore, in recent years, more and more research works have been devoted to designing lithography-free planar thin-film structural color filters, which can be easily scaled up by using vacuum deposition or electrodeposition systems.[28-30]

A widely used thin-film configuration to generate vibrant colors is a Fabry-Pérot (F-P) resonator comprising two metallic mirrors separated by an optically transparent dielectric[31] or a highly absorbing semiconductor medium,[32] in which constructive interferences occur at a certain wavelength, leading to a narrow transmission peak or reflection valley.[33, 34] As a result, the F-P cavity resonance-based color filters generally produce color systems consisting of additive primary colors, i.e., RGB (red, green, blue),[35-37] in the transmission mode; and subtractive primary colors, i.e., CMY (cyan, magenta, yellow),[32, 38, 39] in the reflection mode. In the color space, however, the color gamut of CMY is much smaller than that of RGB, largely hindering the various applications of reflective color filters.[40] Therefore, many efforts have been made recently to design high-purity RGB reflective colors using planar thin-film structures.[8, 41-43] For example, Ghobadi et al. achieved vivid RGB reflective color filters by optimizing the thickness of each layer in a tandem metal-insulator-metal-insulator-semiconductor (MIMIS) multi-cavity structure comprised of Al, zinc oxide (ZnO), and germanium (Ge) materials.[44] Yang et al.[45] and Banerjee et al.[46] reported similar RGB reflective colors but with simpler asymmetric F-P cavity structures consisting of an anti-reflection (AR) overlayer, an absorber layer, a spacer layer, and a

reflective mirror from the top to the bottom. However, it is noteworthy that all these RGB reflective color filters exhibit relatively poor color purity due to the inadequate absorption outside the targeted reflection color range. We proposed a general strategy of using ultrathin bilayer lossy media as effective ideal absorbers to enhance the purity of reflective structural colors in a classic and simple dielectric-absorber-dielectric-metal (DADM) thin-film structure.[47] Although highly pure RGB reflective colors have been demonstrated to verify the effectiveness of this method, the design process of searching for suitable absorber combinations to satisfy the ideal complex refractive index of the absorber layer[48] over a broad wavelength range of nontargeted colors is very complicated and challenging.

In this work, we report a simpler approach for producing high-purity reflective structural colors by incorporating an ultrathin organic dye layer with targeted color appearance into optical cavity structure. The enhanced optical absorptions of the colored dye layer caused by strong cavity resonances can effectively suppress the reflection within the unwanted wavelength range, thus significantly improving the purity of the desired reflective colors. We demonstrated that highly-saturated blue and red reflective color filters with high angular tolerance up to ±60° can be achieved by embedding a very thin layer of blue and red dyes, respectively, and the same method can be extended to other colors. Note that the thickness of the dye layer used is typically less than 30 nm, which is about two orders of magnitude thinner than that used in the conventional colored dye-only coating. Moreover, unlike the typical organic dye-based color coating that can be easily degraded by UV light, our fabricated device exhibits excellent optical stability under accelerated UV exposure test for 15 days, which is equivalent to ~10-year sunlight exposure. This is possible due to the negligible UV absorption inside the dye layer in our design. Based on the proposed method in

this work, the design process of structural colors is much simplified and a desired color of high purity can be easily realized by incorporating a thin dye film of the same color into an optical cavity without the need for an extensive search for the ideal absorbing materials, thereby opening up new revenues for wide applications of structural colors.

Results and discussion

Figure 1a depicts a schematic view of the proposed high-purity blue colored design by using a thin perylenetetracarboxylic bis-benzimidazole (PTCBI) layer, which is a blue colored dye. The entire structure, from the top to the bottom, is composed of a 60 nm TiO_2 AR overlayer, a 15 nm absorber layer of nickel (Ni), a 27 nm thin PTCBI layer, a 60 nm TiO_2 spacer layer, and an Al reflective mirror. The PTCBI underneath the Ni layer acts as both an additional absorber and a spacer layer at the same time, forming a new Ni-PTCBI composite absorber in this DADM structure. The total thickness of PTCBI and the bottom TiO_2 spacer layer corresponds to the half-wave optical thickness of the wavelength at 460 nm, ensuring high reflectance in the blue color range. Moreover, the interference effects excited in this asymmetric F-P resonator result in strong optical absorption of the composite absorber at the other unwanted wavelengths. Figure 1b plots the simulated reflection spectrum (the blue solid curve) of the designed blue color filter based on the Ni-PTCBI composite absorber at normal incidence, presenting a good agreement with the measured spectrum (the blue dashed curve). The reflection beyond 500 nm is greatly suppressed and a reflection peak at the wavelength of 451 nm with a high intensity of ~73% is achieved, which lead to the high-purity and high-brightness blue color displayed in the inset of Figure 1b. As a comparison, the simulated reflection spectrum (the black dashed curve) of a blue color filter based on a single Ni

absorber is also presented in Figure 1b. Here, the TiO_2 spacer layer is re-optimized as 83 nm and the thicknesses of the other layers are fixed. Obviously, the reflection within the nontargeted color range (i.e., 500 ~ 800 nm) is not well suppressed when only using the Ni as the absorbing layer, which consequently compromises the final color purity as shown on the CIE 1931 chromaticity diagram in Figure 1c. In contrast, the structure based on Ni-PTCBI composite absorber exhibits a much improved color purity as its coordinate is very close to the edge of the diagram. The color coordinates calculated from both the simulated (0.150, 0.060) and measured (0.153, 0.069) data of the proposed high-purity blue color are fairly close to the standard blue point (0.150, 0.060) used in liquid crystal displays. By analyzing the absorption in each layer for these two devices as plotted in Figure S1 (Supporting information), it is found that the residual reflection of ~ 10% outside the blue color range in the Ni-based color filter is further suppressed by the strong optical absorption of PTCBI incorporated into this asymmetric F-P resonator. Figure 1d compares the absorption spectra of the PTCBI layer in the blue color device and a single PTCBI with the same thickness on a glass substrate. It is evident that the absorption of PTCBI at long wavelengths is significantly enhanced by the excited F-P cavity resonance, which also well explains the suppressed reflection of the high-purity blue colored device based on Ni-PTCBI composite absorber outside the blue color range. It is interesting to notice that the PTCBI layer embedded in the DADM device shows a reduced absorption at short wavelengths (especially for the wavelength <450 nm) compared with a single PTCBI on the glass substrate, which contributes to the high reflectance of the targeted color. The reduction of absorption in the UV range will also benefit the lifetime of the organic dye, as will be discussed later.
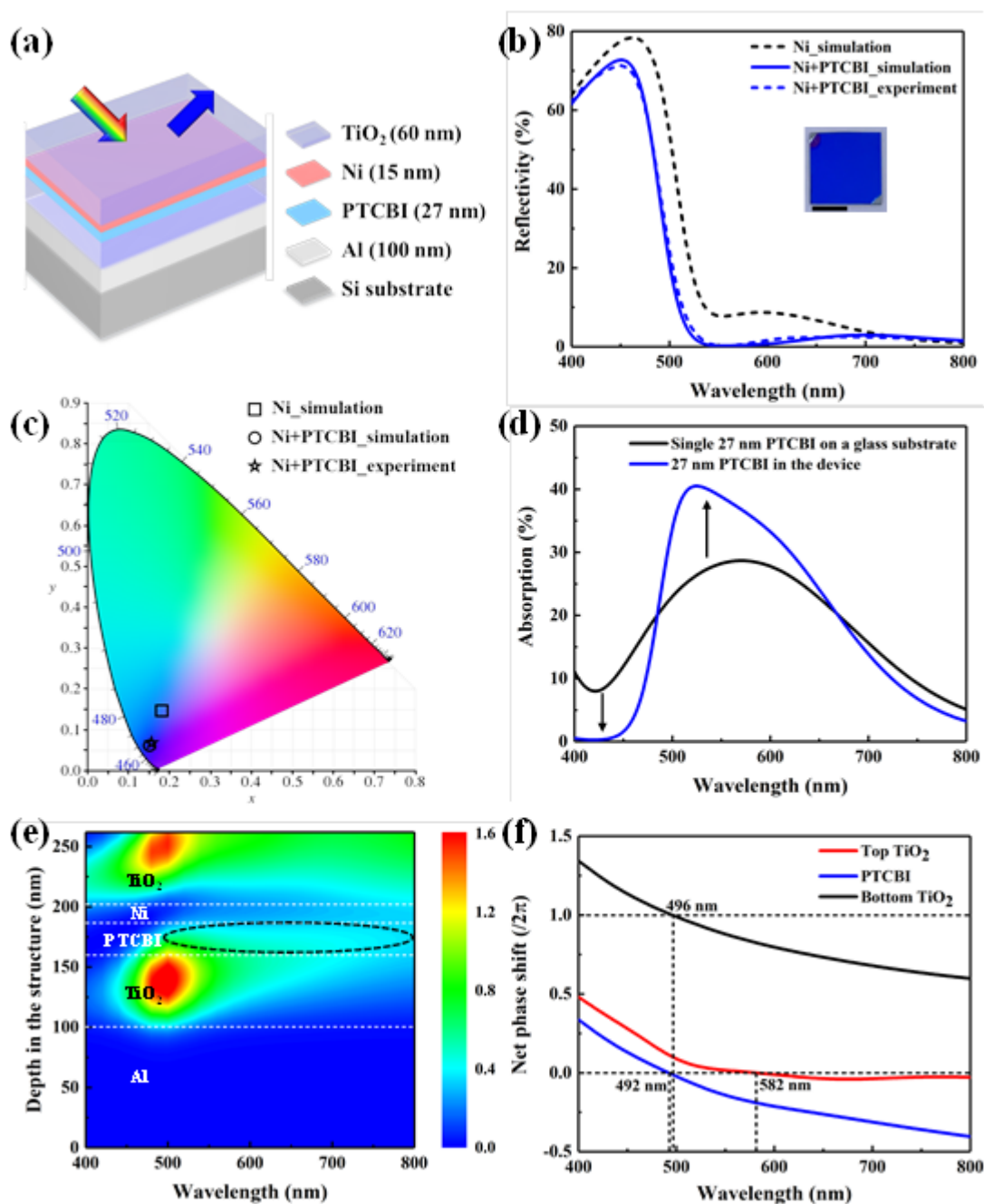
Figure 1. (a) The schematic diagram of the proposed high-purity blue reflective color filter using a Ni-PTCBI composite absorber. **(b)** Comparison of the simulated and measured reflection spectra of blue color filters employing the single Ni absorber and the Ni-PTCBI composite absorber. The inset shows a photograph of the fabricated blue color device on a silicon substrate (Scale bar: 1.0 cm). **(c)** The calculated color coordinates corresponding to all the reflection spectra shown in (b) on the CIE

1931 chromaticity diagram. (d) Comparison of the absorption spectrum of the PTCBI layer in the proposed blue color device to the absorption profile of a single 27 nm PTCBI on a glass substrate. (e) The wavelength-dependent electric field distribution inside the whole structure of the proposed blue color filter employing the Ni-PTCBI composite absorber. (f) Calculated net phase shifts in the PTCBI, top and bottom TiO$_2$ layers as a function of the wavelength for the device.

Both the enhanced absorption at wavelengths >500 nm and reduced absorption in the blue color range of the PTCBI layer can be clearly understood by studying the electric field distribution inside the device based on the Ni-PTCBI composite absorber. As shown in Figure 1e, strong electric field in the PTCBI layer can be observed at wavelength >500 nm as highlighted by the black dotted circle, directly resulting in the efficient optical absorption outside the blue color range as displayed in Figure 1d. The electric field intensities in the Ni-PTCBI composite film are very weak in the short wavelength region <450 nm, leading to the lower absorption loss of the PTCBI layer embedded in the DADM structure compared to that of a single PTCBI film deposited on the glass substrate. It is interesting to note that although the electric field inside the PTCBI layer is relatively strong in the wavelength range of 450 ~ 500 nm, the absorption inside the PTCBI layer is counterintuitively low, which ensures the high reflectivity of the final blue color. This is because of the intrinsically low absorption coefficient of PTCBI within the blue color range, which can be easily inferred from the blue colored appearance of a thick PTCBI dye, i.e., it absorbs light at longer wavelengths. In other words, the high-purity blue color is generated by magnifying the intrinsically high absorption at long wavelength and low absorption at short wavelength of PTCBI in the optical resonant cavity. To further verify the function of the thin blue colored dye in the structural color, we designed another high-purity blue color filter employing the

Ni-PTCBI composite absorber, in which the thickness of Ni was decreased to 10 nm (See more details in Figure S2, Supporting information). As expected, it also exhibits much higher color purity than the Ni-based color filter. Moreover, the PTCBI in this device exhibits a greater absorption enhancement at the unwanted wavelengths (>500 nm) compared with that in the proposed blue color filter employing a Ni (15 nm)-PTCBI composite absorber, further emphasizing the contribution of the PTCBI to the final color purity. The above discussion clearly indicates that a dye having the same color as the final targeted color of the DADM structure is preferred when extending this method in achieving other colors. In addition, the proposed method has great flexibility in the material selection of each layer (especially the absorber) in the DADM structure. As presented in Figure S3, colors of similar purity can be easily achieved when using different absorbing materials, dielectric, and reflective layers with the same dye films. In Figure 1f, the net phase shifts, which involve two reflection phases at both the top and bottom interfaces and the accumulated propagation phase within the layer, are plotted for the PTCBI and the top and bottom TiO_2 layers to reveal the resonant locations. As illustrated by the black and blue curves in the figure, two closely positioned F-P cavity resonance modes are excited within the bottom lossless TiO_2 (@ 496 nm) and the lossy PTCBI (@ 492 nm) layers when the net phase shift is equal to a multiple of 2π, which are well-consistent with the locations of the confined electric field inside these two layers and significantly enhance the absorption at long wavelengths in the PTCBI. The AR resonance occurs inside the top TiO_2 layer @ 582 nm as displayed by the red curve in Figure 1f, where the net phase shift is equal to 0, effectively reducing the broadband reflection outside the blue color range. The F-P resonances and AR resonance contribute together to the enhanced light

absorption in the Ni-PTCBI composite absorber at the unwanted wavelengths (500 ~ 800 nm) and create a perfect absorption peak at 554 nm.
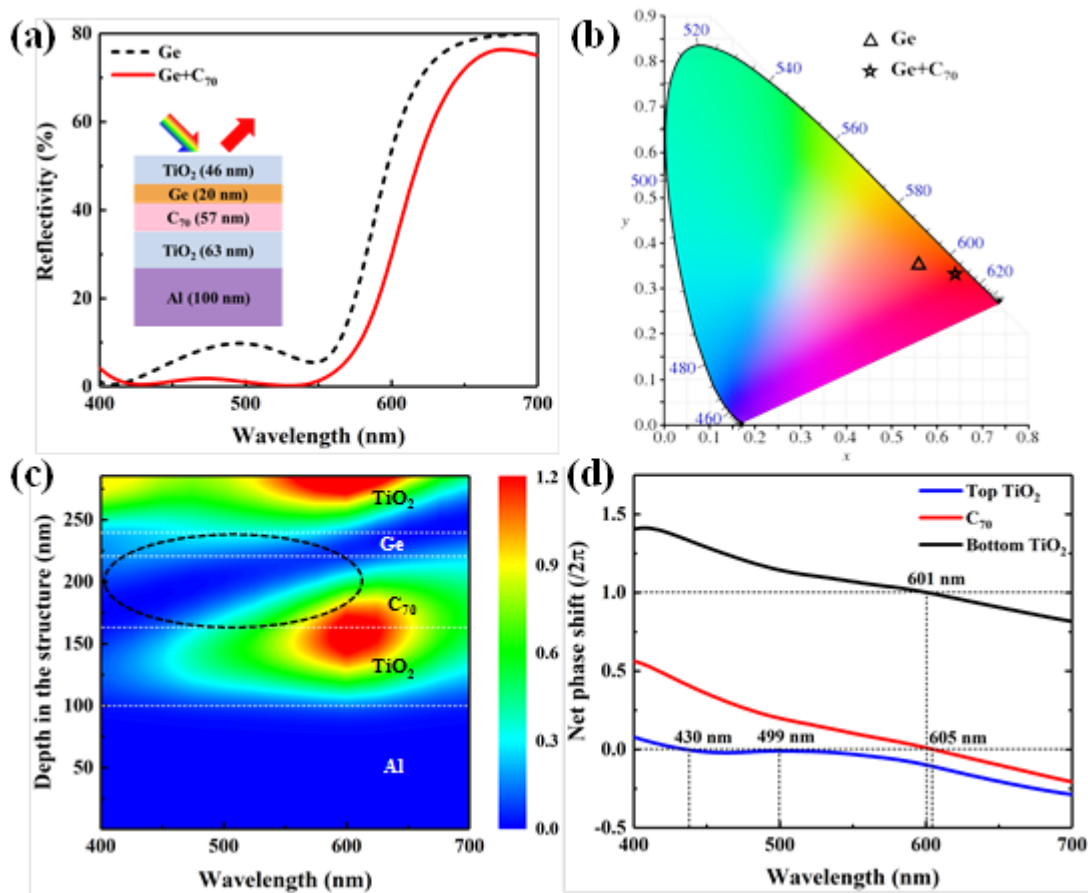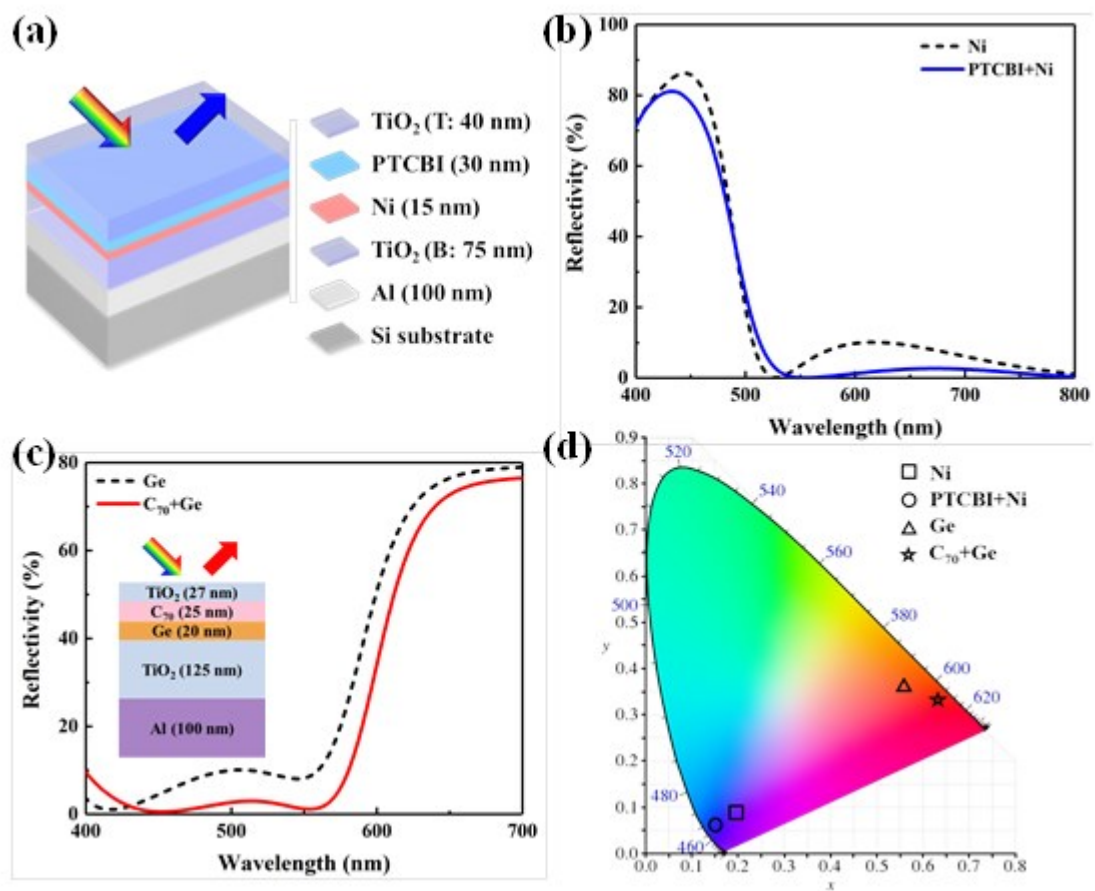

Figure 2. (a) Comparison of the simulated reflection spectra of red color filters based on a single Ge absorber and a Ge-C$_{70}$ composite absorber. The schematic view of the proposed high-purity red reflective color filter is shown in the inset. (b) The calculated color coordinates from the reflection spectra in (a) described on the CIE 1931 chromaticity diagram. (c) The electric field distribution as functions of wavelength and depth inside the red color filter based on the Ge-C$_{70}$ composite absorber. (d) The calculated net phase shifts, which include the two reflection phase shifts and the propagation phase shift, inside the C$_{70}$, top and bottom TiO$_2$ layers.

As mentioned above, this method can be extended to the generation of different colors. To verify this, a high-purity red reflective color filter is also demonstrated by employing a Ge-C_{70} composite absorber, in which a thin red dye layer of C_{70} fullerene is placed underneath the Ge layer. **Figure 2**a compares the simulated reflection spectra of the red color filters using the Ge-C_{70} composite absorber (the red solid curve, see the detailed schematic diagram in the inset) and the single Ge absorber (the black dashed curve, replacing the C_{70} with a 125 nm-thick TiO_2 layer) at normal incidence. Obviously, the color filter based on the Ge-C_{70} composite not only creates a peak reflection of ~77% at the wavelength of 676 nm, but also exhibits much improved light absorption at shorter wavelengths compared with the Ge-based structure, effectively suppressing the light reflection in the unwanted wavelength range. As displayed on the CIE 1931 chromaticity diagram in Figure 2d, the color coordinate of the proposed red color filter using the composite absorber (0.639, 0.331) is very close to the standard red color point (0.640, 0.330), showing significantly enhanced color purity than the one using the single Ge absorber. The same working principles that are used to explain the blue color filter can also be applied to the proposed red colored structure. Figure 2c provides the wavelength-dependent electric filed distribution inside the whole structure of the proposed red color filter employing the Ge-C_{70} composite absorber. Obviously, the strong electric field in the Ge-C_{70} composite absorber appears at wavelength <600 nm as highlighted by the black dotted circle, directly resulting in the efficient light absorption and the suppressed reflection at the short wavelengths. In the long-wavelength range (600 ~ 700 nm), weak and strong electric field distribution can be observed in the Ge and C_{70} layers, respectively. Due to the very small extinction coefficient (k) of C_{70} beyond 600 nm as shown in Figure S11 (Supporting information), the light absorption inside the Ge-C_{70} composite

absorber is fairly low, thereby ensuring the high reflectivity of the red color. The net phase shifts inside the C_{70}, top and bottom TiO_2 layers of the red color device are plotted in Figure 2d to reveal the resonant locations. As illustrated by the red and black curves, two closely positioned F-P cavity resonances are excited within the C_{70} layer (@605 nm) and the bottom TiO_2 layer (601 nm) when the net phase shift is equal to a multiple of 2π, which is consistent with the location of the strongly confined electric field in these two layers and results in the strong short-wavelength absorption of the C_{70} layer. Multiple AR resonances are created at 430 and 499 nm inside the top TiO_2 layer (the blue curve), which effectively reduce the broadband reflection outside the red color range. The F-P and AR resonances function together leading to the enhanced light absorption in the Ge-C_{70} composite absorber at the unwanted wavelengths (400 ~ 600 nm) and creating two perfect absorption peaks at 429 nm and 530 nm, respectively. Figure S4 in the supporting information compares the absorption spectra of the C_{70} layer in the proposed red color device and a single C_{70} on a glass substrate. It is worth noting that the absorption at short wavelengths of the C_{70} layer inside the DADM resonator structure is not enhanced as expected as most of the absorption occurs at the 20 nm-thick Ge layer due to its high loss. However, the contribution of enhanced light absorption at unwanted short wavelengths of the red dye layer resulting from the excited F-P cavity resonances is indispensable, and can be clearly validated when reducing the thickness of the Ge layer or replacing Ge with a less absorptive layer of Ag (See more details in Figure S5, Supporting information). Therefore, the addition of thin red dye in the F-P cavity leads to the improved color purity of the proposed DADM structure.

Figure 3. (a) The schematic diagram of the designed high-purity blue reflective color filter employing a PTCBI-Ni composite absorber. (b) Comparison of the simulated reflection spectra of blue color filters using the single Ni absorber and the PTCBI-Ni composite absorber. (c) Comparison of the simulated reflection spectra of red color filters based on the single Ge absorber and the C_{70}-Ge composite absorber. The inset shows the schematic view of the designed filter. (d) Illustration of color coordinates calculated from all the reflection spectra shown in (b) and (c) on the CIE 1931 chromaticity diagram.

High-purity colors can also be achieved by placing the colored dye film on the top of the absorber layer, which consequently enhances the light absorption at the unwanted wavelengths inside the thin dye layer by exploiting the AR resonance. The proposed high-purity blue color filter employing a PTCBI-Ni composite absorber is schematically

illustrated in **Figure 3**a. In this case, a 30 nm-thick PTCBI layer above the Ni layer acts as both an additional absorber and part of the AR layer at the same time. The total thickness of PTCBI and the top TiO_2 AR layer corresponds to the quarter-wave optical thickness of the wavelength of 610 nm for suppressing red reflection.[47] The simulated reflection spectrum of the blue colored structure based on the PTCBI-Ni composite absorber at normal incidence is plotted in Figure 3b (the blue solid curve), exhibiting a peak reflection of ~ 81% at the wavelength of 434 nm and strong light absorption over the broad long wavelength range of 500 ~ 800 nm. As a comparison, for the blue color filter based on a single Ni absorber, in which a 69 nm-thick TiO_2 film is used as the top AR overlayer and the other layers remain the same, the reflection at long wavelengths is not totally suppressed as illustrated by the black dashed curve in Figure 3b. As a result, the color purity of the blue structural filter based on the single Ni absorber is much worse than that of the structure using the PTCBI-Ni composite absorber. Similarly, placing the red dye film on the top of the absorber layer can also produce highly pure red reflective color in a DADM structure. In Figure 3c, the simulated reflection spectra of the red color filters employing a C_{70}-Ge composite absorber (the red solid curve, the inset shows the detailed structural parameters) and a single Ge absorber (the black dashed curve) are displayed. It can be seen that strong reflections (>75%) from 600 nm to 700 nm are achieved for both red colored structures, while the light absorption below 600 nm is significantly enhanced by using the C_{70}-Ge composite absorber compared with the red color filter based on the single Ge absorber. In order to evaluate the purity of all the blue and red color filters, the corresponding color coordinates are described on the CIE 1931 chromaticity diagram in Figure 3d. Clearly, the color filters based on composite absorbers with additional dye layers exhibit much improved color purity compared

to the devices using a single absorber layer. Besides, the color coordinates of the proposed color filters using composite absorbers (blue (0.153, 0.061) and red (0.632, 0.333)) are fairly close to the standard blue and red colors, indicating their high purity. The blue color device is taken as an example to understand the mechanism of the enhanced light absorption at the unwanted wavelengths after adding a dye film above the absorber layer, which is presented in Figure S6 (Supporting information). The enhanced absorption at long wavelengths of the PTCBI layer in the blue color filter caused by the excited multiple AR resonances further improve the purity of the blue reflective color. In addition, the thickness of PTCBI is adjustable in a wide range of 20 ~ 45 nm to achieve high-purity blue color filter, as discussed in Figure S7 (Supporting information). In principle, high-purity green reflective colors also can be realized by using suitable green colored dyes.
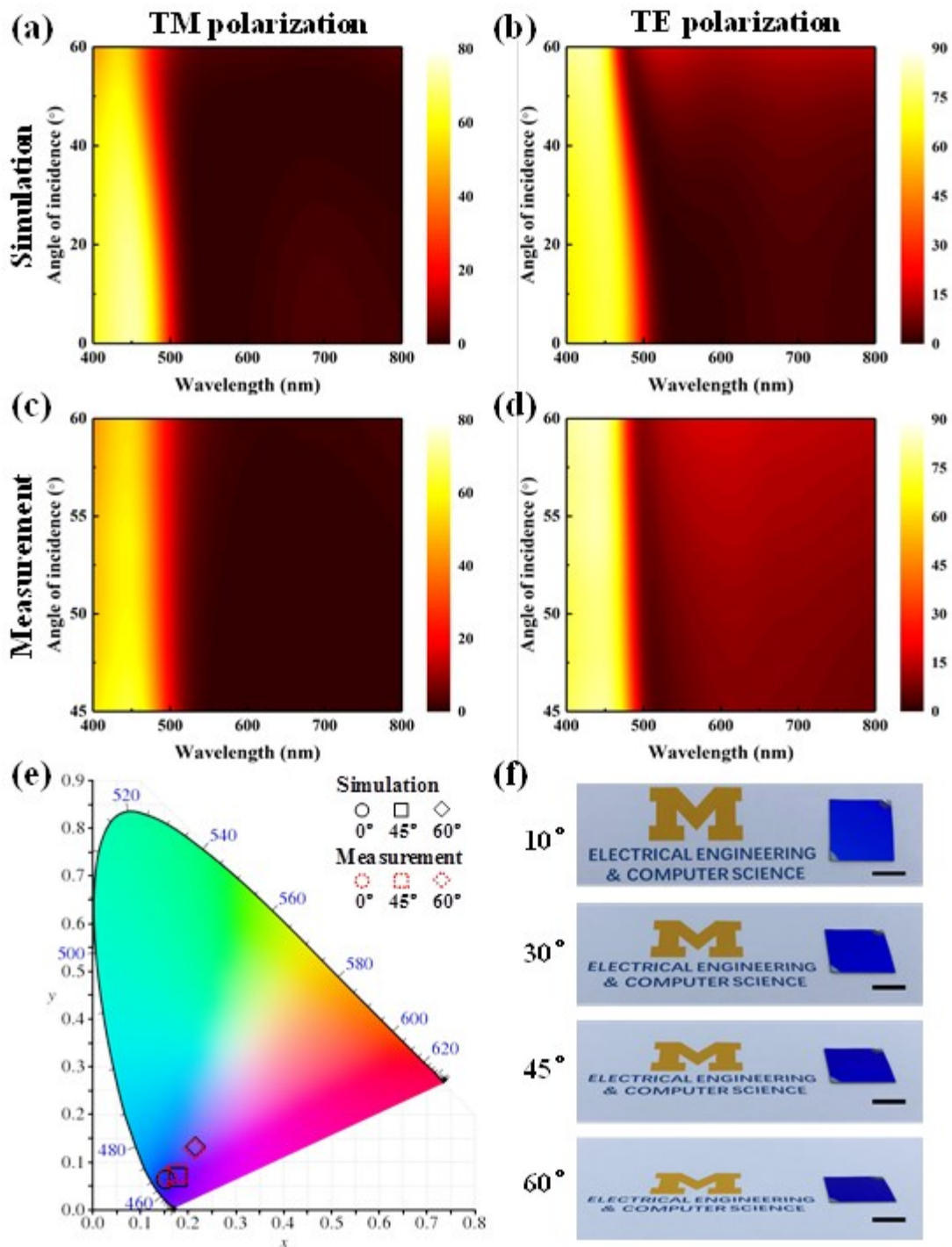
Figure 4. (a) and (b) The simulated angle-resolved reflection spectra of the proposed blue color filter employing the Ni-PTCBI composite absorber under TM and TE polarizations. (c) and (d) Measured angular behaviors corresponding to those in (a) and (b). (e) Visualization of the color change with the

incident angle on the CIE 1931 chromaticity diagram. (f) Photographic images of the fabricated blue color device taken with the ambient light at oblique incidence of 10°, 30°, 45° and 60°. The scale bars are 1.0 cm.

To investigate the angular dependency of the proposed high-purity color filters, the angle-resolved reflection spectra of the blue color device based on the Ni-PTCBI composite absorber were calculated and measured for both transverse magnetic (TM) and transverse electric (TE) polarizations, as illustrated in **Figure 4**a-d. Obviously, the simulation results are very consistent with the measured results and a high angular insensitivity up to $\pm 60°$ is observed regardless of polarizations as indicated by the relatively flat dispersion curves in the plots, which is a direct result of the high indices of the materials utilized in our structure. High index material reduces the angle of light refraction inside the film stack, leading to reduced resonance shift when the incident angle of light is increased.[49] Figure 4e presents the color change with the incident angle up to 60° on the CIE 1931 chromaticity diagram. The closely located color coordinates at different incident angle clearly indicate the great angle-robust appearance of the proposed blue color filter, which can be further proved by the photographs of the fabricated sample taken at different viewing angles, as displayed in Figure 4f. Similarly, the designed blue color filter employing the PTCBI-Ni composite absorber and the other two red reflective color filters based on Ge-C_{70} and C_{70}-Ge composite absorbers are also expected to exhibit a high angular tolerance up to $\pm 60°$ based on the theoretical calculations (See more details in Figure S8 from the supporting information).
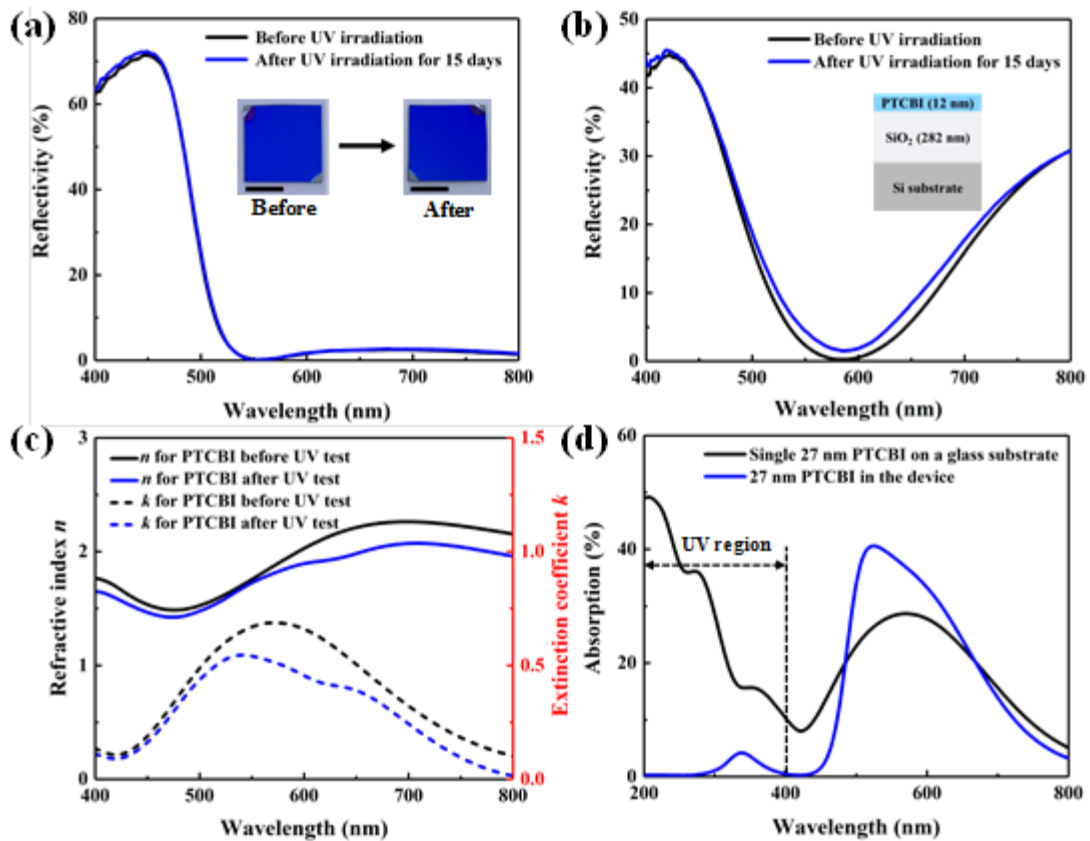
Figure 5. (a, b) Comparison of the measured reflection spectra of the fabricated blue color filter based on the Ni-PTCBI composite absorber (a) and a reference sample (b) before and after UV irradiation for 15 days. The insets in (a) display the optical images of the blue device before and after UV test (Scale bar: 1.0 cm). The schematic view of the reference sample shown as the inset in (b). (c) Comparison of the measured complex refractive indices of PTCBI (in the reference sample) before and after UV test. (d) Comparison of the simulated UV-visible absorption spectra of PTCBI before and after being integrated into the blue colored structure.

Considering that organic dyes usually suffer from short life-time issues, an accelerated UV exposure test was carried out at room temperature to evaluate the stability of the fabricated blue color filter based on the Ni-PTCBI composite absorber. The blue device and a reference sample (12 nm-thick PTCBI deposited on a silica substrate) were placed directly

below a UV lamp with the irradiation intensity of 4.5 mW/cm^2 at a distance of ~ 5 cm. Their

measured reflection spectra before and after UV irradiation for 15 days are shown in **Figure 5**a and 5b. It can be seen that the optical property of the blue device is almost unchanged and

the optical images inserted in Figure 5a show a constant color appearance, indicating the

excellent color stability of the blue device after UV test. Considering that the irradiation

intensity of the sunlight in UV region is ~ 0.01 mW/cm^2, the UV test results indicate that the

fabricated blue color filter can survive more than 10 years under sunlight irradiation. For the

reference sample (the schematic view is provided in Figure 5b), the absorption is slightly

decreased after UV irradiation. The complex refractive indices of PTCBI before and after UV

test are calibrated and provided in Figure 5c, which shows both the refractive index and

extinction coefficient of PTCBI reduce after UV exposure, especially in long-wavelength

region. Based on the extracted refractive indices, the optical responses of 27 nm-thick PTCBI

on a glass substrate before and after UV test are calculated in Figure S9 in the supporting

information, exhibiting a significant difference. Therefore, integrating PTCBI into the F-P

resonator can not only improve the purity of the reflective color, but also greatly extend the

lifetime of the organic dye. Compared to the single PTCBI on the glass substrate, the

enhanced optical stability of PTCBI in the blue device can be attributed to its negligible

optical absorption in UV region, as illustrated in Figure 5d. Similarly, the UV absorption of

PTCBI in the blue color filter based on the PTCBI-Ni composite absorber is much lower than

that of the single PTCBI on the glass substrate (See more details in Figure S10, Supporting

information). This effect can be understood by referring to the design principle laid out for

DADM in Ref. [47]: around the peak reflection wavelength λ_c, the E-field of the light at the

absorber layer location should satisfy $E(\lambda_c) \approx 0$ to minimize absorption loss and achieve high

reflectivity. Correspondingly, around the wavelength $\lambda_c/2$ located in the UV region, the E-field intensity around the absorber layer position is also close to zero. Note that this principle can be generalized for any other reflection colors when the same colored dyes are introduced in the cavity structures, thereby the lifetime of the dyes should always be enhanced. Such increase of lifetime can be regarded as another huge benefit of using structural color designs as compared with just using the organic dyes for colored coatings. In addition, the emission property of organic dyes, generally, should not be a concern for achieving high-purity reflective colors unless the fluorescent quantum yield of the dye is strong; but if the quantum yield is low, e.g. only 10%, the effect on the color purity of the devices is quite minimal. Moreover, the fluorescent property of dyes degrades fast when exposed to oxygen and moisture. Therefore, for long term color coating application, any fluorescence effect can be safely neglected. For the dye materials used in this work, the fluorescent emission of PTCBI is in the NIR range,[50] and although C_{70} has fluorescent emission at the wavelengths > 700 nm,[51] its quantum yield is very low ($\sim 5.7 \times 10^{-4}$). Therefore, their the fluorescent properties have no effects on the reflection performance and color purity of the proposed blue and red colored devices.

Conclusions

In summary, a simple strategy of incorporating a thin dye layer into the resonant cavity of a classic DADM structure is described in this work for the generation of high-purity reflective structural colors. A dye having the same color as the final targeted color of the structure is used in the design, and its intrinsically low absorption in the desired wavelength range and high absorption at other wavelengths are amplified by the excited cavity

resonances, which leads to the high reflection of final color with improved color purity. Note that the design of high-purity reflective colors in this work is different from that in our previous work of using bilayer metal absorbers,[47] which involves a complicated searching process for suitable absorber combinations to satisfy the derived complex refractive index of the ideal absorber layer within nontargeted color range. In this work, the design process of high-purity structural colors can be much simplified by directly using the organic dye materials with targeted color appearance as it does not have a stringent requirement on the absorber selection. Due to the high refractive indices of the materials used in the devices, the proposed structural colors also show great angular insensitivity up to ±60° regardless of the polarization state of incident light. Compared to other types of structural colors generated by sub-wavelength nanopatterns, the proposed layered structures can be easily scaled up to mass production as multiple materials can be easily done by one deposition run in an evaporator without breaking the vacuum, or by using continuous roll to roll deposition in an industrial manufacturing setting. In addition, the fabricated device exhibits an excellent color stability in the accelerated UV exposure test, which results from the significantly reduced UV absorption of the dye layer when integrated into the F-P resonator. The facile strategy presented here has not only simplified the design process of high-purity structural colors by avoiding the need for searching for the ideal absorbing materials in a DADM structure, but also greatly extended the lifetime of organic dyes, thereby holding great potential to be used in various applications including color displays, optical decorations, and optical detections.

Methods

Device Fabrication: The designed blue reflective color filter based on the metal-dye composite absorber was fabricated by e-beam evaporation and thermal evaporation on a silicon substrate. Al, TiO$_2$, and Ni films were deposited at room temperature with a rate of 3 Å/s when the e-beam evaporator chamber was pumped down to a base pressure of 4×10^{-6} Torr. PTCBI was deposited by a thermal evaporator at a rate of 0.5 Å/s at a vacuum base pressure of less than 5×10^{-6} mbar.

Simulation and Measurement: Optical simulations for calculating the reflection/absorption/transmission spectra, normalized electric field distributions, and net phase shifts were performed using the transfer matrix method. The reflection spectrum of the fabricated blue color filter at normal incidence was measured by a thin-film measurement instrument (F20, Filmetrics) integrated with a spectrometer and a white light source. The measured angle-resolved reflection spectra were obtained with a spectroscopic ellipsometer (M-2000, J. A. Woollam). The same ellipsometer was used to calibrate the complex refractive indices of Al, Ag, Ge, Ni, chromium (Cr), titanium (Ti), tungsten (W), zinc sulfide (ZnS), silicon nitride (Si$_3$N$_4$), TiO$_2$, and PTCBI used in the optical simulations, and the results are provided in Figure S11 (Supporting information). The complex refractive index of C$_{70}$ fullerene in the wavelength range of 400 ~ 700 nm was taken from the data reported by Cao et al.[52]

Acknowledgments

Notes

The authors declare no competing financial interest.

References

[1] Z. M. Yang, Y. Q. Chen, Y. M. Zhou, Y. S. Wang, P. Dai, X. P. Zhu, H. G. Duan, *Adv. Opt. Mater.* **2017**, *5*, 1700029.

[2] K. Kumar, H. G. Duan, R. S. Hegde, S. C. W. Koh, J. N. Wei, J. K. W. Yang, *Nat. Nanotechnol.* **2012**, *7*, 557.

[3] F. Cheng, J. Gao, T. S. Luk, X. D. Yang, *Sci. Rep.* **2015**, *5*, 11045.

[4] X. L. Zhu, W. Yan, U. Levy, N. A. Mortensen, A. Kristensen, *Sci. Adv.* **2017**, *3*, e1602487.

[5] C. G. Ji, Z. Zhang, T. Masuda, Y. Kudo, L. J. Guo, *Nanoscale Horiz.* **2019**, *4*, 874.

[6] K. T. Lee, J. Y. Lee, S. Y. Seo, L. J. Guo, *Light Sci. Appl.* **2014**, *3*, e215.

[7] Y. B. Qiu, L. Zhan, X. Hu, S. Y. Luo, Y. X. Xia, *Displays* **2011**, *32*, 308.

[8] J. Hong, E. Chan, T. Chang, T. C. Fung, B. Hong, C. Kim, J. Ma, Y. L. Pan, R. Van Lier, S. G. Wang, B. Wen, L. X. Zhou, *Optica* **2015**, *2*, 589.

[9] H. Liu, H. Yang, Y. R. Li, B. X. Song, Y. F. Wang, Z. R. Liu, L. Peng, H. Lim, J. Yoon, W. Wu, *Adv. Opt. Mater.* **2019**, *7*, 1801639.

[10] S. Koyama, Y. Inaba, M. Kasano, T. Murata, *IEEE Trans. Electron Devices* **2008**, *55*, 754.

[11] J. G. Park, S. H. Kim, S. Magkiriadou, T. M. Choi, Y. S. Kim, V. N. Manoharan, *Angew. Chem. Int. Ed.* **2014**, *53*, 2899.

[12] K. T. Lee, C. G. Ji, D. Banerjee, L. J. Guo, *Laser Photonics Rev.* **2015**, *9*, 354.

[13] S. D. Rezaei, R. J. H. Ng, Z. G. Dong, J. F. Ho, E. H. H. Koay, S. Ramakrishna, J. K. W. Yang, *ACS Nano* **2019**, *13*, 3580.

[14] A. S. Roberts, A. Pors, O. Albrektsen, S. I. Bozhevolnyi, *Nano Lett.* **2014**, *14*, 783.

[15] H. Wang, X. L. Wang, C. Yan, H. Zhao, J. W. Zhang, C. Santschi, O. J. F. Martin, *ACS Nano* **2017**, *11*, 4419.

[16] Z. B. Li, A. W. Clark, J. M. Cooper, *ACS Nano* **2016**, *10*, 492.

[17] Y. K. R. Wu, A. E. Hollowell, C. Zhang, L. J. Guo, *Sci. Rep.* **2013**, *3*, 1194.

[18] A. F. Kaplan, T. Xu, L. J. Guo, *Appl. Phys. Lett.* **2011**, *99*, 143111.

[19] X. M. Goh, R. J. H. Ng, S. H. Wang, S. J. Tan, J. K. W. Yang, *ACS Photonics* **2016**, *3*, 1000.

[20] Y. Nagasaki, M. Suzuki, I. Hotta, J. Takahara, *ACS Photonics* **2018**, *5*, 1460.

[21] S. Sun, Z. X. Zhou, C. Zhang, Y. S. Gao, Z. H. Duan, S. M. Xiao, Q. H. Song, *ACS Nano* **2017**, *11*, 4445.

[22] T. Wood, M. Naffouti, J. Berthelot, T. David, J. B. Claude, L. Metayer, A. Delobbe, L. Favre, A. Ronda, I. Berbezier, N. Bonod, M. Abbarchi, *ACS Photonics* **2017**, *4*, 873.

[23] M. L. Tseng, J. Yang, M. Semmlinger, C. Zhang, P. Nordlander, N. J. Halas, *Nano Lett.* **2017**, *17*, 6034.

[24] Y. X. Zhang, Q. Zhang, X. Ouyang, D. Y. Lei, A. P. Zhang, H. Y. Tam, *ACS Nano* **2018**, *12*, 9913.

[25] K. Xiong, D. Tordera, G. Emilsson, O. Olsson, U. Linderhed, M. P. Jonsson, A. B. Dahlin, *Nano Lett.* **2017**, *17*, 7033.

[26] L. Shao, X. L. Zhuo, J. F. Wang, *Adv. Mater.* **2018**, *30*, 1704338.

[27] A. B. Evlyukhin, S. M. Novikov, U. Zywietz, R. L. Eriksen, C. Reinhardt, S. I. Bozhevolnyi, B. N. Chichkov, *Nano Lett.* **2012**, *12*, 3749.

[28] C. G. Ji, S. Acharya, K. Yamada, S. Maldonado, L. J. Guo, *ACS Appl. Mater. Interfaces* **2019**, *11*, 29065.

[29] Z. M. Yang, Y. M. Zhou, Y. Q. Chen, Y. S. Wang, P. Dai, Z. G. Zhang, H. G. Duan, *Adv. Opt. Mater.* **2016**, *4*, 1196.

[30] J. Ma, J. C. Wang, Z. D. Hu, Z. D. Zhang, L. Pan, A. Di Falco, *AIP Adv.* **2019**, *9*, 11.

[31] Z. Y. Li, S. Butun, K. Aydin, *ACS Photonics* **2015**, *2*, 183.

[32] K. T. Lee, S. Seo, J. Y. Lee, L. J. Guo, *Adv. Mater.* **2014**, *26*, 6324.

[33] M. A. Kats, F. Capasso, *Laser Photonics Rev.* **2016**, *10*, 735.

[34] C. S. Park, V. R. Shrestha, S. S. Lee, D. Y. Choi, *Sci. Rep.* **2016**, *6*, 25496.

[35] C. S. Park, V. R. Shrestha, S. S. Lee, E. S. Kim, D. Y. Choi, *Sci. Rep.* **2015**, *5*, 8467.

[36] K. T. Lee, S. Y. Han, H. J. Park, *Adv. Opt. Mater.* **2017**, *5*, 1700284.

[37] J. H. Han, D. Kim, T. W. Lee, Y. Jeon, H. S. Lee, K. C. Choi, *ACS Photonics* **2018**, *5*, 3322.

[38] C. G. Ji, C. Y. Yang, W. D. Shen, K. T. Lee, Y. G. Zhang, X. Liu, L. J. Guo, *Nano Res.* **2019**, *12*, 543.

[39] C. Y. Yang, K. N. Mao, W. D. Shen, B. Fang, X. Fang, X. Zhang, Y. G. Zhang, X. Liu, *Appl. Phys. Lett.* **2016**, *109*, 241104.

[40] D. H. Kim, Y. J. Yoo, J. H. Ko, Y. J. Kim, Y. M. Song, *Opt. Mater. Express* **2019**, *9*, 3342.

[41] C. G. Ji, K. T. Lee, L. J. Guo, *Opt. Lett.* **2019**, *44*, 86.

[42] J. Kim, H. Oh, M. Seo, M. Lee, *ACS Photonics* **2019**, *6*, 2342.

[43] S. D. Rezaei, J. Ho, A. Naderi, M. T. Yaraki, T. Wang, Z. G. Dong, S. Ramakrishna, J. K. W. Yang, *Adv. Opt. Mater.* **2019**, *7*, 1900735.

[44] A. Ghobadi, H. Hajian, M. C. Soydan, B. Butun, E. Ozbay, *Sci. Rep.* **2019**, *9*, 290.

[45]C. Y. Yang, W. D. Shen, Y. G. Zhang, K. Li, X. Fang, X. Zhang, X. Liu, *Sci. Rep.* **2015**, *5*, 9285.

[46]D. Banerjee, *US 9658375 B2*, **2017**.

[47]Z. M. Yang, C. G. Ji, D. Liu, L. Guo, *Adv. Opt. Mater.* **2019**, 1900739.

[48] D. Liu, H. T. Yu, Z. Yang, Y. Y. Duan, *Nano Res.* **2016**, *9*, 2354.

[49]C. G. Ji, K. T. Lee, T. Xu, J. Zhou, H. J. Park, L. J. Guo, *Adv. Opt. Mater.* **2017**, *5*, 1700368.

[50] E. I. Haskal, Z. Shen, P. E. Burrows, S. R. Forrest, *Phys. Rev. B* **1995**, *51*, 4449.

[51] A. A. Tukhbatullin, G. L. Sharipov, A. R. Bagautdinova, *RSC Adv.* **2016**, *6*, 26531.

[52]J. Cao, Z. Zhan, L. T. Hou, Y. B. Long, P. Y. Liu, W. J. Mai, *Appl. Opt.* **2012**, *51*, 5718.

Table of contents text (adom.202000317R1)
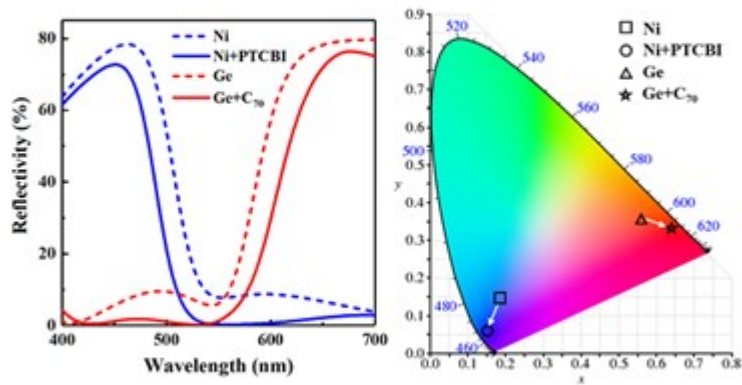
A simple approach that incorporates an ultrathin dye film into a classic dielectric-absorber-dielectric-metal multilayered structure is presented to produce high-purity reflective colors. The enhanced optical absorptions of the colored dye layer as a result of the strong cavity resonances can effectively suppress the reflection within the unwanted wavelength range, thus significantly improving the purity of the desired reflective colors.